Ain Shams Engineering Journal 16 (2025) 103789

Contents lists available at ScienceDirect

Ain Shams Engineering Journal

journal homepage: www.sciencedirect.com

Full Length Article

Iron-modified biochar from fermented grain residues for enhanced oxytetracycline degradation via periodate activation

Tiehong Song [a], Ying Zhang [a], Hongyan Wei [a], Ying Wang [b], Yanjiao Gao [c,*]

[a] Urban Construction College, Changchun University of Architecture and Civil Engineering, Changchun 130607, PR China
[b] Key Laboratory of Songliao Aquatic Environment, Ministry of Education, Jilin Jianzhu University, Changchun 130118, PR China
[c] College of Civil Engineering and Architecture, Liaoning University of Technology, Jinzhou 121001, PR China

ARTICLE INFO

Keywords:
Oxytetracycline
Periodate
Fermented grain residues
Advanced oxidation processes
Iron-modified biochar

ABSTRACT

The frequent presence of antibiotics like oxytetracycline (OTC) in aquatic environments has raised significant concerns owing to their potential to cause antibiotic resistance genes and ecological risks, demanding efficient and sustainable remediation methods. This study developed a novel iron-modified biochar (4MBC800) derived from fermented grain residues to activate periodate (PI) for OTC degradation. The biochar was prepared via pyrolysis and characterized by various instruments, revealing a well-developed porous structure and high specific surface area. Under operating conditions (OTC = 20.4 mg/L, 4MBC800 = 1.1 g/L, PI = 3.3 g/L, t = 150 min), 92.1% of OTC was effectively removed. Radical quenching experiments and HPLC-MS analysis identified $^{\bullet}OH$, $^{\bullet}O_2^-$, and $^1O_2$ as the dominant reactive species driving OTC degradation through three distinct pathways. The 4MBC800/PI system demonstrated robust catalytic performance, reusability, and adaptability across different water matrices without generating toxic byproducts. This work provides new insights into the design of waste-derived catalysts for periodate-based advanced oxidation processes in antibiotic-contaminated water treatment.

1. Introduction

The expanding demands for disease prevention and treatment have led to the extensive use of antibiotics worldwide, particularly in high-population regions [1]. The persistence of antibiotic residues in aquatic ecosystems promotes the proliferation of antibiotic-resistant bacteria, posing significant risks to ecological and human health [2]. Classified as emerging contaminants by WHO guidelines, antibiotics require priority control. However, conventional wastewater treatment processes designed for removing biochemical oxygen demand (BOD), nitrogen, and phosphorus exhibit limited efficiency in degrading most antibiotics. Hence, there is an urgent need to develop advanced technologies for effective antibiotic removal.

Oxytetracycline (OTC), a widely used tetracycline antibiotic, features a linearly fused four-cyclohexane-ring structure that resists natural degradation in water [3,4], making it a common model pollutant in degradation studies. Advanced oxidation processes (AOPs) rely on in situ generation of reactive oxygen species (ROS) that exhibit strong oxidative capacity toward organic pollutants [5]. Conventional AOPs include hydroxyl radical ($^{\bullet}OH$, E^0 = 1.8–2.7 V)-based systems such as UV/H_2O_2 and Fenton (Fe^{2+}/H_2O_2) processes [6], as well as sulfate radical ($SO_4^{\bullet-}$, E^0 = 2.5–3.1 V)-based systems, in which persulfate ($S_2O_8^{2-}$) or peroxymonosulfate (HSO_5^-) is activated to generate $SO_4^{\bullet-}$ [6,7]. While $^{\bullet}OH$-based oxidation is highly pH-dependent and non-selective, $SO_4^{\bullet-}$-based oxidation operates over a wider pH range and targets electron-rich organic compounds [8,9]. Nonetheless, $SO_4^{\bullet-}$ is susceptible to interference from background anions (e.g., Cl^-, HCO_3^-, CO_3^{2-}), limiting its practicality in real water matrices [10].

Recently, periodate (IO_4^-, E^0 = 1.6 V)-based AOPs have gained attention due to their ability to generate multiple ROS (e.g., $^{\bullet}OH$, $^1O_2$, $IO_3^{\bullet}$, $IO_4^{\bullet}$) via tailored activation methods [11]. Unlike conventional AOPs, periodate-based systems perform effectively over a broad pH range [12,13]. Iodate (IO_3^-), the main reduction product, is non-toxic and easily removable through precipitation [14]. Moreover, iodine radicals (e.g., $IO_3^{\bullet}$ and $IO_4^{\bullet}$) preferentially oxidize electron-rich organic moieties via electron transfer mechanisms [15]. Various strategies have been explored to activate periodate (PI), including carbon activation, UV irradiation [16,17], and metal-based activation [18–20]. Biochar (BC), a carbonaceous material, possesses high surface area, modifiable surface chemistry, and environmental compatibility. Fermented grain

* Corresponding author.
E-mail address: tmgyj@lnut.edu.cn (Y. Gao).

https://doi.org/10.1016/j.asej.2025.103789
Received 21 July 2025; Received in revised form 19 September 2025; Accepted 22 September 2025
Available online 30 September 2025

residues from liquor production, can be pyrolyzed into BC for activating PI in organic pollutant degradation [21–23]. Furthermore, modifying BC with transition metals can enhance its catalytic performance [21–24]. Iron-functionalized BC demonstrates superior catalytic activity for PI activation due to the synergistic effect between iron species and the carbon matrix, which facilitates electron transfer and ROS generation [25–27].

In this study, iron-doped BC was synthesized from fermented grain residues through pyrolysis and employed as a novel activator of PI toward OTC decontamination. This study aims to: (i) characterize the physicochemical properties of various BCs prepared under different prepare conditions; (ii) analyze the efficacy of various BCs in activating PI for OTC removal; (iii) clarify the OTC degradation mechanism and identify OTC transformation products; (iv) evaluate the reusability of optimal BC, its performance in different water matrices, and the toxicity of degradation products. This study provides a dual waste valorization strategy that utilize waste fermented grain residues to produce BC in removing antibiotic from wastewater.

2. Materials and methods

2.1. Chemical reagents

Sodium periodate ($NaIO_4$), potassium ferrate (K_2FeO_4), sulfuric acid (H_2SO_4), sodium hydroxide (NaOH), sodium chloride (NaCl), sodium bicarbonate (Na_2CO_3), and sodium nitrate ($NaNO_3$) were provided by Sinopharm Group Chemical reagent Co., LTD. Oxytetracycline ($C_{22}H_{24}N_2O_9$), humic acid ($C_9H_8Na_2O_4$), *tert*-butanol ($C_4H_{10}O$), p-benzoquinone ($C_6H_4O_2$), and furfuryl alcohol ($C_5H_6O_2$) were obtained from Shanghai Maclin Biochemical Technology Co., LTD. These chemicals were analytical reagents except for *tert*-butanol which was chemically pure. The contaminant solution used in the experiment was prepared by dissolving needed chemicals into ultra-pure water.

2.2. Preparation of biochar

The biomass raw material for preparing BC was waste fermented grain residues. BC was prepared by high temperature pyrolysis. The fermented grain residues were cleaned with ultra-pure water and dried for 24 h in a drying oven at 80 ℃. The dried fermented grain residues were made into powder by grinder, and 80 mesh powder was screened for pyrolysis. The powders were pyrolyzed in a nitrogen-purged tube furnace at 100 ml/min N_2 flow rate and heated at a heating rate of 10 ℃/min, with the final temperature 500 ℃, 650 ℃, and 800 ℃. These BCs were named BC500, BC650, and BC800, corresponding to pyrolysis temperatures of 500 ℃, 650 ℃, and 800 ℃, respectively. Next, one-step pyrolysis method was used to prepare the modified BC. Eighty mesh grain residues powder (10 g) and K_2FeO_4 powder (2 g or 4 g) were put into ultra-pure water, and the solution was stirred and mixed for 24 h, and then left for 6 h. The mixed solution was vacuum-filtered and left with filter residues, which was dried at 80 ℃ for 12 h. The dried residues were crushed, screened via 80 mesh filter, and finally were pyrolyzed in a tube furnace. The pyrolysis conditions were the same as those for the preparation of unmodified BC. According to the final pyrolysis temperature (500 ℃, 650 ℃, and 800 ℃) and the quality of doped K_2FeO_4 (2 g, 4 g), the modified BC were recorded as 2MBC500, 2MBC650, 2MBC800, 4MBC500, 4MBC650, and 4MBC800, respectively.

2.3. Characterization of biochar

Biochar characterization was performed with multiple analytical techniques. Morphological evaluation was obtained by scanning electron microscopy (SEM, MERLIN Compact, ZEIS, Germany), and elemental compositions were determined via energy-dispersive X-ray spectroscopy (EDS, equipped on SEM). Surface area and porosity were analyzed using a specific surface area analyzer (ASAP2460, Micromeritics, USA). Chemical bonds of elements were characterized by X-ray photoelectron spectroscopy (XPS, Thermo Scientific K-Alpha+, USA), crystalline phase was identified with X-ray diffraction (XRD, Ultima IV, Rigaku, Japan), the vibrations of all bonds were detected through Fourier transform infrared spectroscopy (FTIR, Frontier, Perkin Elmer, USA), and carbon structure analysis was carried out by Raman spectroscopy (LabRAM HR Evolution, HORIBA JY, France).

2.4. Experimental procedures

The adsorption experiments of various BCs for OTC were conducted using beakers at room temperature (T = 25 ± 1 ℃). First, BC (100 mg) was introduced into a 250 mL-beaker containing 100 mL of OTC solution (20.4 mg/L, pre-adjusted pH = 3), then magnetic stirring was applied to initiate the adsorption process. Samples were taken out (at 10, 30, 60, 90, 120, 150 min) and immediately transferred to a spectrophotometer for absorbance measurement, and the values were subsequently converted to OTC concentrations based on a linear calibration curve.

Catalytic experiments were conducted to examine the effectiveness of various BC-activated PI for OTC degradation. 100 ml of OTC solution (20.4 mg/L, pre-adjusted pH = 3) was put into a beaker, followed by the addition of BC (1.1 g/L) and PI (3.3 g/L), and the catalytic reaction began under magnetic stirring. The sampling and measuring followed the same method as aforementioned adsorption experiments. The procedure of the influence factor experiments was similar to that of the catalytic experiments, except that the specific reaction parameters were varied in the dosage. The specific experimental parameters were indicated in the captions of the corresponding results figures.

2.5. Analytical methods

The OTC concentration measurements were performed via a spectrophotometer (TU-1810, Beijing Purkinje Co., Ltd., China) at 355 nm. The standard calibration curve for OTC concentration versus absorbance is shown in Fig. 1a. UV spectra of the OTC solution and a treated sample are exhibited in Fig. 1b. OTC solution (before reaction) possessed two absorption peaks (260 nm and 355 nm). However, the absorption peak of the reacted solution shifted at 260 nm, so this experiment employed a wavelength of 355 nm for OTC sample detection. Additionally, OTC degradation product identification was performed by liquid chromatography-mass spectrometry (Ultimate 3000 UHPLC-Q Exactive, Thermo Scientific, USA).

3. Results and discussion

3.1. Characterization of biochar

Fig. 2 provides SEM images of various BCs (BC500, BC650, BC800, 2MBC500, 2MBC650, 2MBC800, 4MBC500, 4MBC650, 4MBC800). It was found that various BCs formed abundant pore structures due to the cracking and volatilization of the organic components in the fermented grain residues via pyrolysis process. On the images of iron-doped biochar (2MBC500, 2MBC650, 2MBC800, 4MBC500, 4MBC650, 4MBC800), some small crystals were found irregularly distributed in some crevices, aperture openings, and interiors, which were hypothesized to be iron species introduced by iron-dopping. An EDS equipped on SEM detected the content of elements in various BCs, as shown in Table 1. EDS spectra of various BCs are shown in Appendix I. It can be seen that trace amounts of element Fe were present in the unmodified BC, while the content of Fe increased significantly in the modified BC. This indicates that Fe was successfully introduced into the BC. Specific surface area of BCs by BET adsorption assay are displayed in Table 2. Among various BCs, 4MBC800 obtained the largest specific surface area of 264 m^2/g. A large specific surface area facilitates the adsorption of oxidants and pollutants, providing sites for activation. In addition, total pore capacity and micropore capacity of 4MBC800 were larger than that

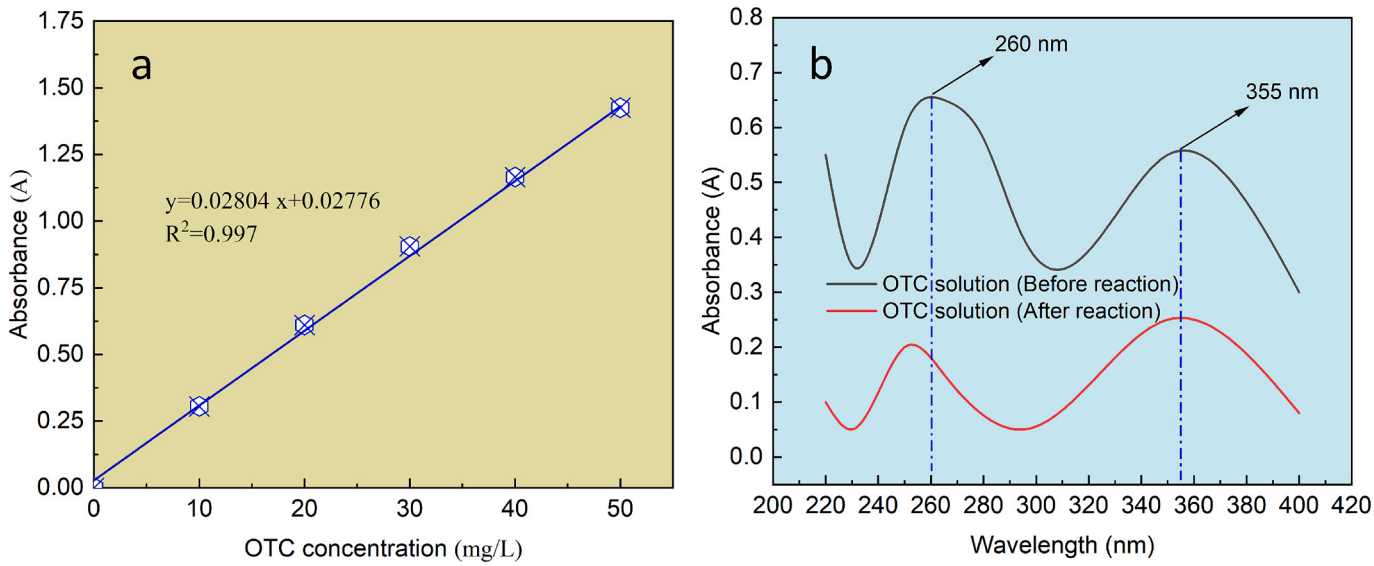

Fig. 1. a: Standard calibration curve between OTC concentration and absorbance; b: UV spectra of the OTC solution and a treated sample.

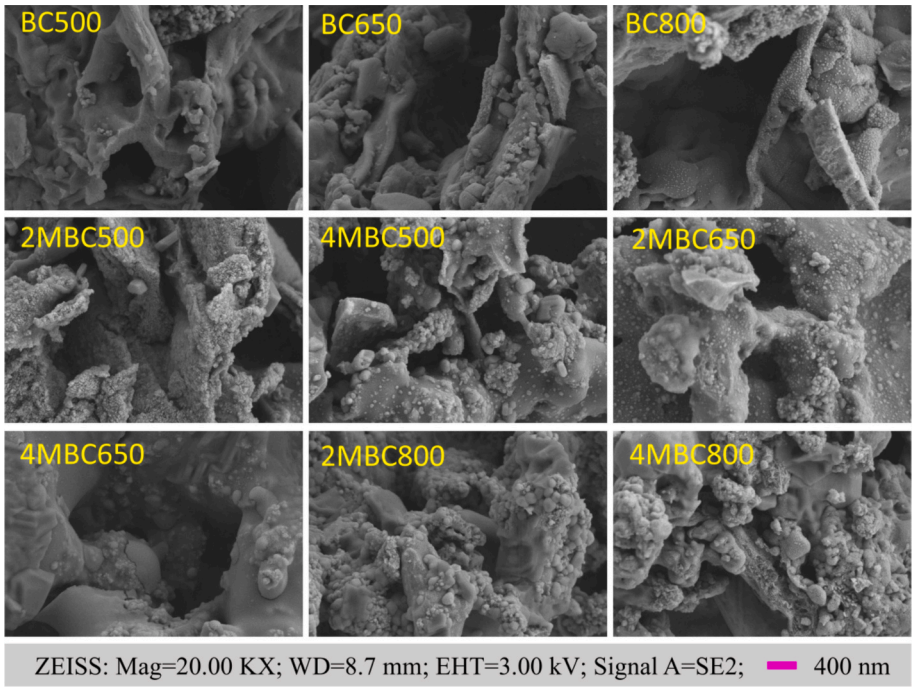

Fig. 2. SEM images of various biochars.

Table 1
Analysis of elemental species and content by EDS.

Element	BC500	BC650	BC800	2MBC500	2MBC650	2MBC800	4MBC500	4MBC650	4MBC800
C	75.84	85.15	83.03	68.82	65.61	40.86	47.80	38.59	21.32
N	5.12	4.24	0.55	2.56	0.00	0.21	0.51	0.00	0.14
O	16.55	8.38	11.50	16.85	8.92	27.99	21.72	23.05	8.88
Na	0.02	0.00	0.03	0.03	0.00	0.05	0.01	0.00	0.07
Mg	0.56	0.11	0.23	0.24	0.07	0.13	0.13	0.16	0.10
Si	1.20	1.53	1.75	2.33	13.57	13.68	5.08	3.62	2.07
K	0.55	0.30	0.50	3.16	9.25	7.54	15.15	6.26	3.76
Ca	0.08	0.06	2.03	0.19	0.00	0.12	0.22	0.25	0.09
Fe	0.07	0.22	0.38	5.83	2.57	9.43	9.38	28.06	63.56
Total	100.00	100.00	100.00	100.00	100.00	100.00	100.00	100.00	100.00

Table 2
Specific surface area and pore characteristics of biochar.

Biochar	Specific surface area (m^2/g)	Surface area of micropore (m^2/g)	Total pore capacity (cm^3/g)	Micropore capacity (cm^3/g)	Average pore size (nm)
BC500	79	62	0.0524	0.0252	2.6
BC650	114	88	0.0603	0.0354	2.1
BC800	260	189	0.1549	0.0885	2.4
2MBC500	219	168	0.1519	0.0994	2.8
2MBC650	215	164	0.1505	0.0995	2.8
2MBC800	215	162	0.1500	0.0960	2.8
4MBC500	229	177	0.1481	0.0961	2.6
4MBC650	225	156	0.1508	0.0849	2.7
4MBC800	264	190	0.1774	0.1072	2.7

of other BCs. Therefore, it is considered that the adsorption performance of 4MBC800 is superior to that of other catalysts, which also provides favorable conditions for catalytic PI. Following SEM, EDS, and BET analysis, we conducted adsorption and degradation performance experiments on various materials to confirm the superiority of 4MBC800 (3.2. Removal of OTC by different systems).

Through adsorption and degradation experiments with various materials, it was determined that 4MBC800 is the optimal catalytic material. Therefore, we conducted further material characterization mainly on 4MBC800.

Fig. 3a and Fig. 3b demonstrate the general XPS spectra of BC800 and 4MBC800, respectively. The two spectra both possessed three distinct absorption peaks, C1s (293.08 eV), O1s (532.08 eV) and N1s (378.28 eV) [28]. Since both BC800 and 4MBC800 were produced by pyrolysis from fermented grain residues, they retained the C, O, and N elements present in the original fermented grain residues. The C and O primarily originated from the organic matter in the fermented grain residues, while the N was mainly derived from proteins, amino acids, and undecomposed yeast residues. Notably, the general XPS spectrum of 4MBC800 appeared an absorption peak of Fe2p, located at 712.08 eV, indicating that Fe was successfully loaded onto the BC. The iron element originated from the K_2FeO_4 reagent used for BC modification. The C1s spectrum (Fig. 3c) showed three absorption peaks, C–C (284.8 eV), C–O (286.2 eV), and C=O (290.71 eV), with the highest intensity was C–C, followed by C–O and C=O. Fig. 3d shows the O1s spectrum, which was fitted into two peaks, C–O (532.48 eV) and C=O (531.54 eV). The main content of O1s was C=O [29]. Generally speaking, the high C=O/C–O ratio favors pollutant removal in the BC/PI system. Fig. 3e is the N1s spectrum, and the two peaks fitted were pyridine N (397.0 eV) and pyrrole N (401.2 eV), with pyrrole N dominating. Fig. 3f fits the peaks of Fe2p, including two major peaks Fe2p3/2 (712.08 eV) and Fe2p1/2 (728.48 eV), and three satellite peaks (716.58 eV, 719.08 eV, and 722.48 eV). It can be seen that Fe primarily occurred as Fe^{3+} and Fe^{2+}. Fig. 3g and Fig. 3h exhibit the XRD patterns of unmodified BC and modified BC. BC500, BC650, and BC800 all showed broad and strong diffraction peaks at 22°, corresponding to the (002) crystal plane of amorphous carbon (Fig. 3g) [30]. Rising pyrolysis temperature (from 500 ℃ to 800 ℃) increased the intensity of the peaks, suggesting that high temperatures could enhance the crystallinity of BC. Fig. 3h shows that diffraction peaks of Fe_2O_3, $FeSiO_3$, Fe and Fe_3O_4 were generated near $2\theta = 30.3°$, 32.9°, 44.6° and 65.0°, respectively [31]. This indicates that the BC was modified by K_2FeO_4 to form various valence states of Fe. FTIR characterization (Fig. 3i) showed that the original BC and modified BC exhibited rich functional group structures. The specific functional groups were O–H (3438 cm^{-1}), C–H (2923 cm^{-1}), C=O (1625 cm^{-1}), C–O (964 cm^{-1}), C–H (574 cm^{-1}), Fe–O (569 cm^{-1}), where the Fe–O of 4MBC800 was evident, suggesting that Fe was successfully loaded onto the 4MBC800 [32]. In Raman spectra (Fig. 3j), the D and G peaks were positioned at 1358 cm^{-1} and 1581 cm^{-1}, respectively. The I_D/I_G elevated from 0.819 to 1.099 as the pyrolysis temperature increased from 500 ℃ to 800 ℃. The D peak represents the defective or disordered carbon in the lattice of C atoms in the BC, while the G peak represents the E2g stretching vibration in the face of sp2 hybridization of C atoms [33]. Usually, the intensity ratio of I_D/I_G can reflect the degree of defects in the BC, with higher values corresponding to more defective BC structures. In the BC studied herein, I_D/I_G increased from 0.819 to 1.099, suggesting that higher pyrolysis temperatures lead to increased structural defects in BC.

3.2. Removal of OTC by different systems

BC exhibits a certain adsorption performance toward pollutants resulting from the large specific surface area and rich microporous architecture. Fig. 4a investigates the adsorption performance of different types of BCs on OTC. It can be observed that the OTC removal rates by BC500, BC650 and BC800 were 22.8 %, 24.7 % and 25.8 %, respectively, within 150 min. This suggests that the adsorption of OTC by the BCs prepared at higher temperature (BC650 and BC800) were better. High-temperature treatment significantly increased BC's specific surface area and pore volume, directly enhancing its adsorption capacity for OTC. It was also found that the adsorption properties of iron modified BCs were enhanced compared to the unmodified BCs. Moreover, the BC with high concentration of iron (4MBC800) in the modification process was more effective in adsorbing OTC than the BC modified with low concentration of iron (2MBC800). 4MBC800 could obtained the maximal OTC removal rate of 43.8 % among various BCs. This may be due to the iron modification of the BC at higher temperatures, which introduces more oxygen-functional groups and enhances the adsorption behavior [34].

Although the BC was able to adsorb a certain amount of OTC, its removal rate did not reach the desired value. Therefore it is necessary to use oxidizing agents to enhance the removal of OTC by the system. Fig. 4b demonstrates the OTC removal under various BC/PI systems. In the case of OTC oxidation by PI alone, OTC removal was able to reach 56 %, which indicates that PI alone can oxidize a portion of OTC based on the mild oxidizing property of PI ($E^0 = 1.6$ V). When the PI system was filled with various BC catalysts, there was a significant increase in the removal of OTC by various BC/PI systems (Fig. 4b) compared to the corresponding adsorption process (Fig. 4a). In the case of unmodified BCs, BC500, BC650 and BC800 were able to remove 81.8 %, 83.6 % and 88.9 % of OTC in the presence of PI, respectively. For iron-modified BCs, 2MBC800 and 4MBC800 were superior, removing 90.1 % and 92.1 % of OTC in PI solution, respectively. This indicates that there is an increase in the removal of OTC in Fe-modified BC with a higher amount of K_2FeO_4 doping. For this reason, the 4MBC800 with the best catalytic effect was chosen for the subsequent experiments. Generally speaking, the adsorption of OTC by biochar is beneficial for its effective degradation. Biochar can concentrate OTC on its surface, creating a locally high concentration that provides more active sites for PI activation. The 4MBC800 catalyst in this experiment exhibits excellent adsorption performance while maintaining good catalytic activity, confirming this observation.

3.3. Mechanism analysis

To identify the ROS generated in the 4MBC800/PI/OTC system, radical trapping experiments were performed using specific scavengers: *tert*-butyl alcohol (TBA) for hydroxyl radicals ($^{\bullet}OH$), p-benzoquinone (p-BQ) for superoxide radicals ($^{\bullet}O_2^-$), and furfuryl alcohol (FFA) for singlet oxygen ($^1O_2$). The kinetic rate constants (k) for the reactions of TBA, p-BQ, and FFA with their corresponding target species ($^{\bullet}OH$, $^{\bullet}O_2^-$, $^1O_2$) are 5.0×10^8 M^{-1} s^{-1}, 0.9×10^9 M^{-1} s^{-1}, 1.2×10^8 M^{-1} s^{-1}, respectively [35–37]. As depicted in Fig. 5, compared to the control group, TBA, p-BQ, and FFA all inhibited OTC degradation to varying degrees, indicating the presence of all three reactive species ($^{\bullet}OH$, $^{\bullet}O_2^-$, $^1O_2$) in the 4MBC800/PI/OTC reaction system. In the control group, the removal rate of OTC reached 92.1 %, while in the groups with addition of TBA, p-BQ, and FFA, the OTC removal rates decreased to 87 %, 59.9 %, and

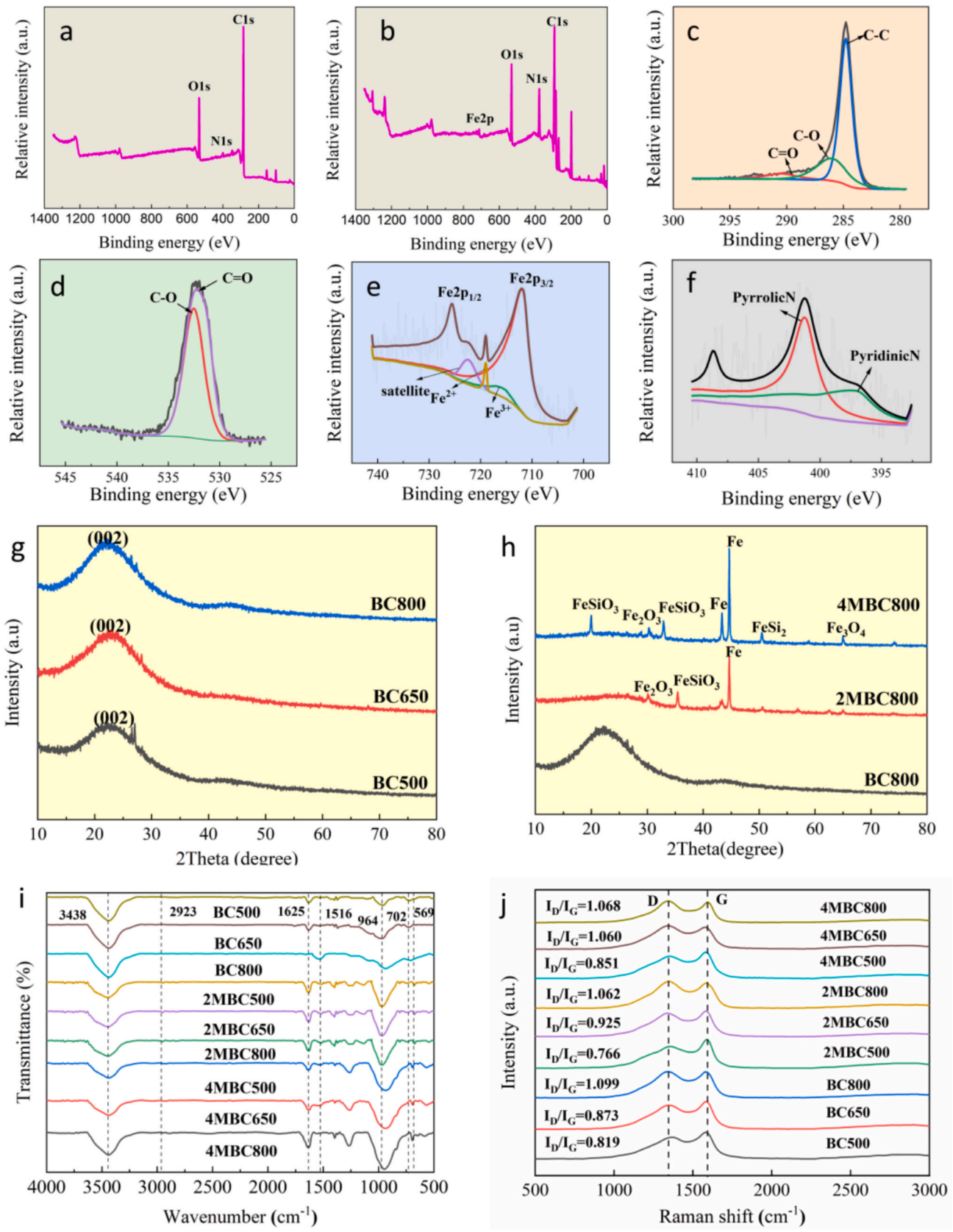

Fig. 3. a: General spectrum of BC800; b: General spectrum of 4MBC800; c: C1s of 4MBC800; d: O1s of 4MBC800; e: Fe2p of 4MBC800; f: N1s of 4MBC800; g: XRD patterns of unmodified BCs; h: XRD patterns of modified BC; i: FTIR spectra of BCs; j: Roman spectra of BCs.

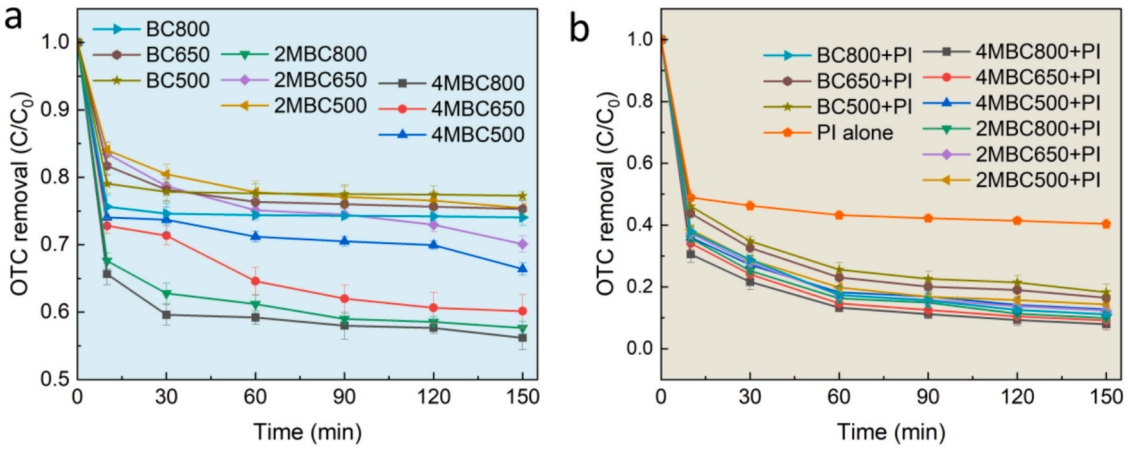

Fig. 4. a: OTC removal of various biochars; b: OTC removal under various biochar/PI systems. [OTC] = 20.4 mg/L, [biochar] = 1.1 g/L, [PI] = 3.3 g/L, T = 25 ℃, pH = 3.

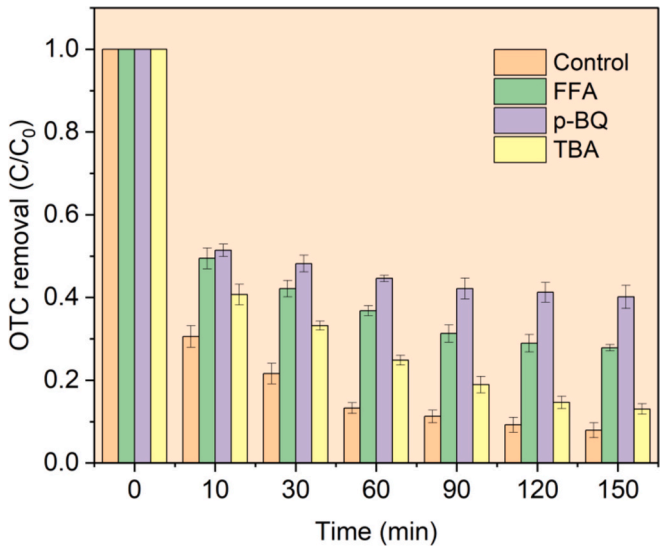

Fig. 5. Effects of different quenchers on OTC removal. [OTC] = 20.4 mg/L, [PI] = 3.3 g/L, [BC] = 1.1 g/L, pH = 3, TBA:PI = 1000:1, [FFA] = 0.2 M, [BQ] = 5 mM.

72.1 %, respectively. In other words, the presence of TBA, p-BQ, and FFA led to a reduction in OTC removal efficiency by 5.1 %, 32.2 %, and 20 %, respectively. These results collectively demonstrate that the three scavengers (TBA, p-BQ, and FFA) inhibited a total of 57.3 % of OTC degradation, indicating the persistent presence of additional reactive species in the system. Elimination analysis conclusively revealed the existence of iodate radicals ($IO_3^{\bullet}$, $IO_4^{\bullet}$) in the 4MBC800/PI/OTC system. Therefore, the elimination of OTC was accomplished through the collaborative work of various reactive species, which may generate through a series of chain reactions (Eqs. 1–8) mediated by iron species and IO_4^-.

$$Fe^0 + 2IO_4^- + H^+ \rightarrow Fe^{2+} + 2IO_3^{\bullet} + 2OH^- \quad (1)$$

$$Fe^{2+} + 2IO_4^- + H_2O \rightarrow Fe^{3+} + IO_3^- + \bullet O_2^- + 2H^+ \quad (2)$$

$$IO_4^- + 2 \bullet O_2^- + H_2O \rightarrow IO_3^- + 2\,{}^1O_2 + 2OH^- \quad (3)$$

$$2 \bullet O_2^- + H_2O \rightarrow H_2O_2 + {}^1O_2 + 2OH^- \quad (4)$$

$$Fe^{3+} + H_2O_2 \rightarrow Fe^{2+} + \bullet O_2^- + 2H^+ \quad (5)$$

$$BC\text{-}OH + IO_4^- \rightarrow BC\text{-}O \bullet + IO_3^{\bullet} + \bullet OH \quad (6)$$

$$BC\text{-}OOH + IO_4^- \rightarrow BC\text{-}OO \bullet + IO_3^{\bullet} + \bullet OH \quad (7)$$

$$IO_4^- + \bullet OH \rightarrow OH^- + IO_4^{\bullet} \quad (8)$$

The possible products of OTC oxidation were determined using HPLC-MS and its degradation routes of OTC were speculated, as depicted in Fig. 6. In pathway I, OTC (m/z = 461) forms the product P1 (m/z = 340) via deamination, deamidation and dehydroxylation, P1 generates P2 (m/z = 285) via ring-opening decarbonylation and dehydroxylation, then P2 undergoes decarbonylation and dehydration to form P3 (m/z = 243), and finally P3 generates P4 (m/z = 193) via ring-opening decarbonylation and demethylation. In pathway II, OTC (m/z = 461) forms the product P5 (m/z = 393) via dehydrogenation and deamidation, P5 deamination, hydrogenation and dehydroxylation forms the product P6 (m/z = 360), P6 generates P7 (m/z = 263) via ring-opening decarbonylation, dehydroxylation and dehydration, and finally P7 generates P8 (m/z = 193) via ring-opening decarbonylation and demethylation. In pathway III, OTC (m/z = 461) generates the product P9 (m/z = 450) by dehydration.P9 is cleaved to P10 (m/z = 393) by demethylation, deamination, dehydration and other reactions, and P11 (m/z = 316) is formed by demethylation and deamidation of P10.

3.4. Evaluation of practical applications

3.4.1. Effects of water quality

In general, in an advanced oxidation system, pH value exerts an important impact on the reaction process. The degradation effects of 4MBC800 toward OTC at three pH values was examined, as shown in Fig. 7. The initial pH of 3, 6, and 9 respectively corresponded to 92.1 %, 88.4 %, and 85.4 % OTC removal in the 4MBC800/PI system. Under acidic conditions (pH = 3), the ≡Fe(II)/≡Fe(III) redox cycle on the iron-modified biochar surface is enhanced, which directly reduces periodate (IO_4^-) to generate highly reactive radicals (e.g., $^{\bullet}OH$ and $IO_3^{\bullet}$), thereby achieving a high OTC removal efficiency [38]. In alkaline conditions, the elevated pH promotes the formation of Fe(OH)/FeOOH precipitates, which coat the active sites on the biochar surface and impede electron transfer [39]. Moreover, under alkaline environments, the oxidation process primarily relies on singlet oxygen ($^1O_2$) or high-valent iron-oxo species ($Fe^{(IV)}$ =O), whose oxidative capacity is inferior to that of free radicals, resulting in lower OTC degradation efficiency [40]. Additionally, in alkaline solutions, OTC undergoes deprotonation (–OH/−NH_2 dissociation), acquiring a negative charge that electrostatically repels the similarly negatively charged 4MBC800/PI surface, thereby reducing interaction probability [41]. Notably, in the 4MBC800/PI system, the

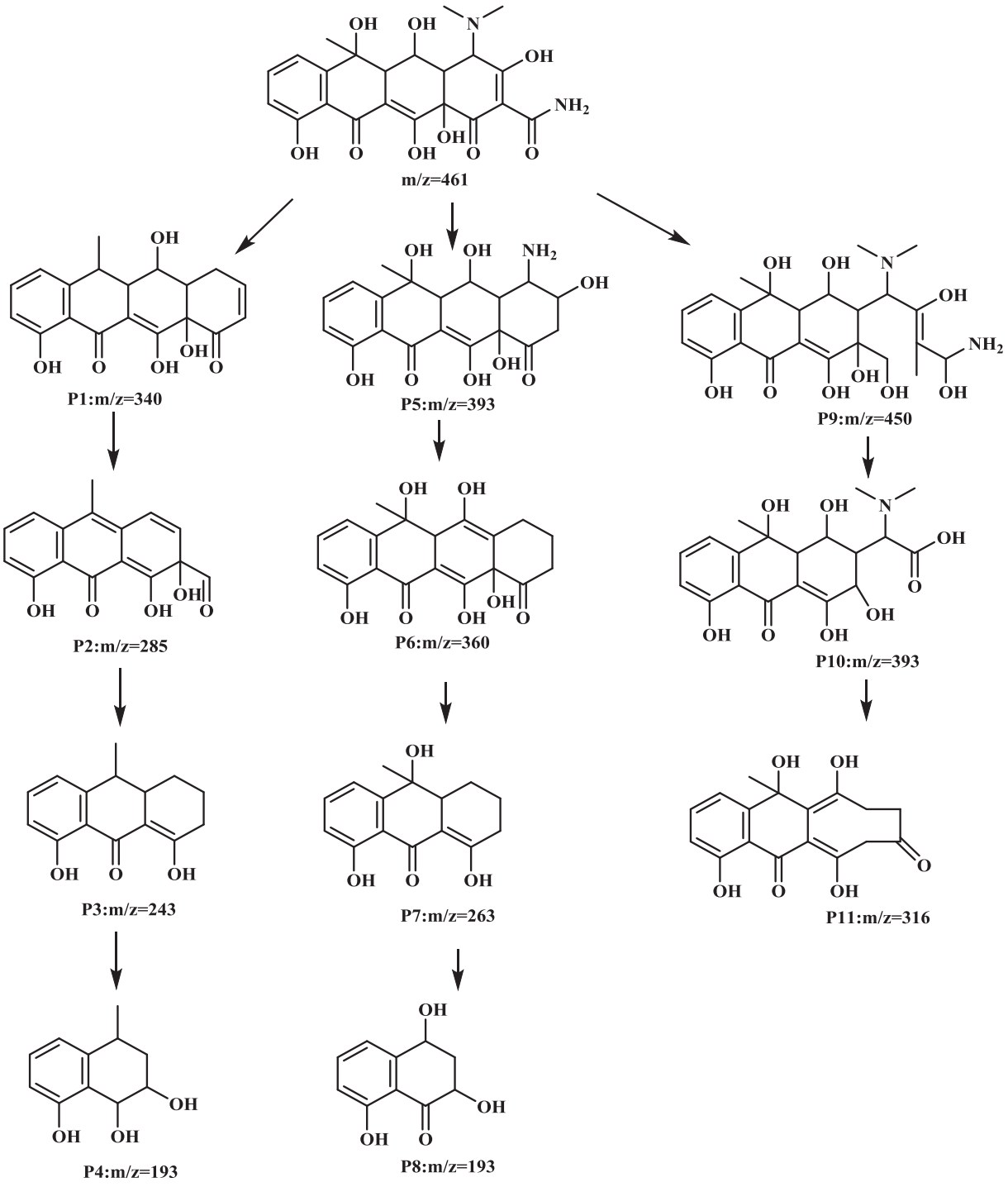

Fig. 6. Possible degradation pathways for OTC.

difference in OTC decontamination efficacy between acidic and alkaline conditions was only 6.7 %, demonstrating strong pH adaptability of the system.

In this study, three representative temperatures (15 ℃, 25 ℃, 35 ℃) were chosen to evaluate their impact on OTC removal performance of the 4MBC800/PI system. The increase in temperature raised the OTC removal rate from 89.5 % to 93.6 % (Fig. 7), indicating that moderate heating had a positive effect. This is attributed to accelerated molecular motion in the heterogeneous system at higher temperatures, which enhanced mass transfer in the 4MBC800/PI system [42]. However, as the tested temperature range was relatively narrow (ambient conditions), no significant improvement in OTC removal efficiency was observed.

In natural water bodies, the occurrence of natural organic matter (NOM) and various anions may significantly influence the degradation of target pollutants in the reaction system. Therefore, this study investigated the individual effects of humic acid (HA, a representative NOM), chloride (Cl^-), nitrate (NO_3^-), and bicarbonate (HCO_3^-) on OTC degradation in the 4MBC800/PI system. At HA 5 mg/L and 10 mg/L, the OTC removal decreased by only 1–3% compared to the control group (Fig. 7), demonstrating that HA at these levels had negligible impact on OTC degradation. Moreover, chloride (Cl^-) and nitrate (NO_3^-) ions were also found to exhibit minimal influence on OTC removal efficiency. These results demonstrate that the 4MBC800/PI system exhibits strong

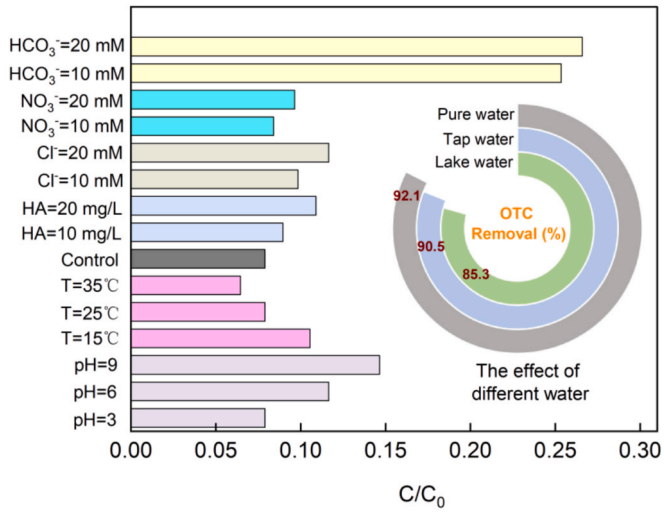

Fig. 7. Effect of water quality conditions on OTC removal. [OTC] = 20.4 mg/L, [PI] = 3.3 g/L, [BC] = 1.1 g/L, pH = 3.

resistance to interference from NOM and common anions. Compared to other anions, HCO_3^- demonstrated significantly stronger inhibition on OTC degradation at both tested concentrations. The presence of HCO_3^- led to a decline in OTC removal efficiency due to two synergistic mechanisms: HCO_3^- increased solution pH, creating less favorable conditions for degradation. As a classic quencher, HCO_3^- directly inhibited reactive oxygen species ($^{\bullet}OH/IO_3^{\bullet}$) through these reactions (Eqs. 9–10):

$$HCO_3^- + \bullet OH \rightarrow CO_3^{\bullet -} + H_2O \quad (9)$$

$$HCO_3^- + IO_3^{\bullet} \rightarrow \text{Inert products} \quad (10)$$

Fig. 7 (inset) compares OTC degradation performance in ultrapure water, tap water, and surface water, revealing a measurable decline in removal efficiency under realistic water matrices. In summary, the experimental results demonstrate that the 4MBC800/PI system exhibits strong resistance to interference from most NOM and anions while maintaining high OTC degradation efficiency in real water matrices. This confirms its excellent applicability and practical potential for actual water treatment applications.

3.4.2. Stability of 4MBC800

To evaluate the reusability of 4MBC800, four cyclic experiments were performed to investigate OTC removal by 4MBC800/PI in each cycle. The results are shown in Fig. 8. It is demonstrated that the OTC removal rates in the four cycles were 89.4 %, 85.9 %, 83.6 %, and 83.2 %, respectively (Fig. 8a). The degradation efficiency exhibited a decreasing trend in each cycle, which may primarily result from the adsorption of intermediate products on the catalyst surface and chemical changes induced by surface oxidation. The adsorption of intermediates could lead to a reduction in active sites and specific surface area, thereby hindering the activation of PI. Additionally, chemical changes on the catalyst surface are a critical factor affecting catalytic performance, as they determine the availability of active sites for PI. During the catalytic process, oxidation of functional groups and carbon structures on the biochar surface may contribute to the decline in removal efficiency. Notably, after the third cycle, the removal rate remained relatively stable. Moreover, in the fourth cycle, the catalyst still maintained a removal rate of over 80 %, demonstrating its favorable reusability. On the other hand, the kinetics of OTC removal over four reuse cycles were simulated to reflect the reaction rate in each cycle, as shown in Fig. 8b. As the number of reuse cycles increased, the degradation rate of OTC followed a second-order kinetic equation, with R^2 values all exceeding 0.93. However, the kinetic constant was the highest in the first reuse cycle, while those for the third and fourth cycles showed a slight decrease. Therefore, from a kinetic perspective, the material's reaction performance remained highly stable.

3.4.3. Toxicity analysis of products

To systematically evaluate the potential ecological toxicity risks of OTC and its degradation intermediates, this study utilized the ECOSAR software, developed by the Chinese Academy of Sciences, to assess both acute toxicity and chronic toxicity in three representative aquatic organisms: fish, daphnia, and algae. Fig. 9 a–c illustrate the logarithmic distribution of acute toxicity, showing that all OTC degradation intermediates exhibit lower ecotoxicity than OTC itself, with most falling into the non-toxic range. Fig. 9 d–f present the chronic toxicity (ChV) analysis, indicating that P2, P6, P7, and P11 are within the non-toxic range, while P4 shows a relatively higher chronic toxicity risk, though still lower than that of OTC. These results demonstrate that the 4MBC800/PI catalytic system not only effectively degrades OTC but also ensures good ecological safety.

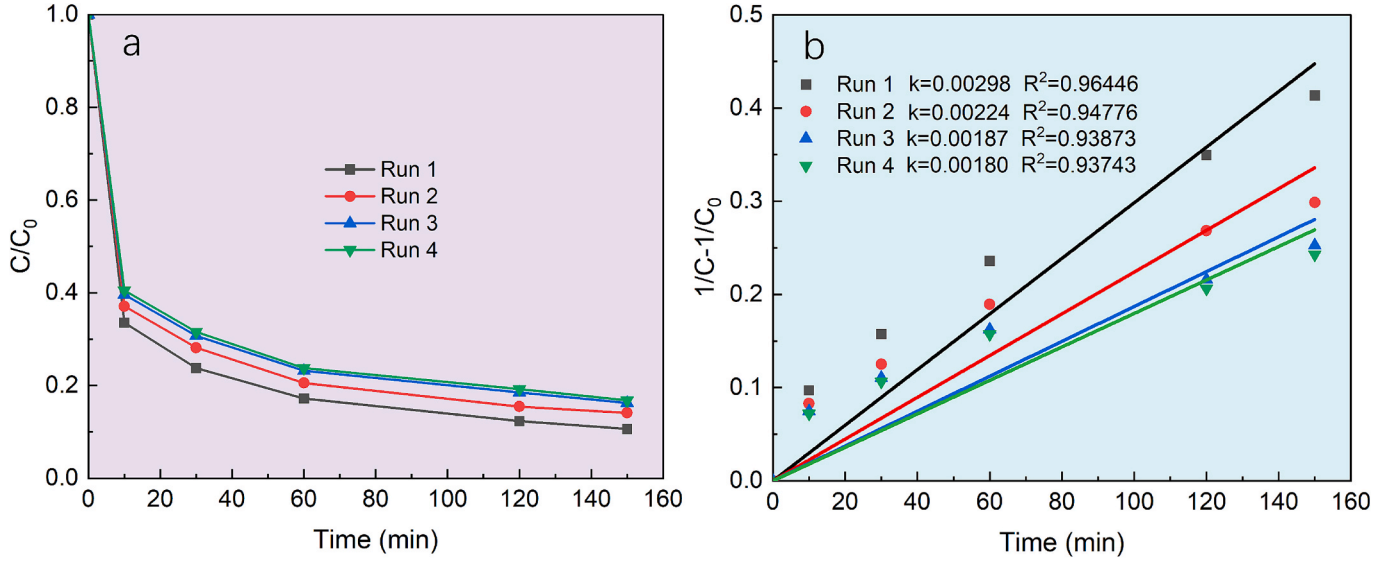

Fig. 8. a: OTC removal with time in four runs reuse; b: OTC removal kinetics in four runs reuse. [OTC] = 20.4 mg/L, [PI] = 3.3 g/L, pH = 3.

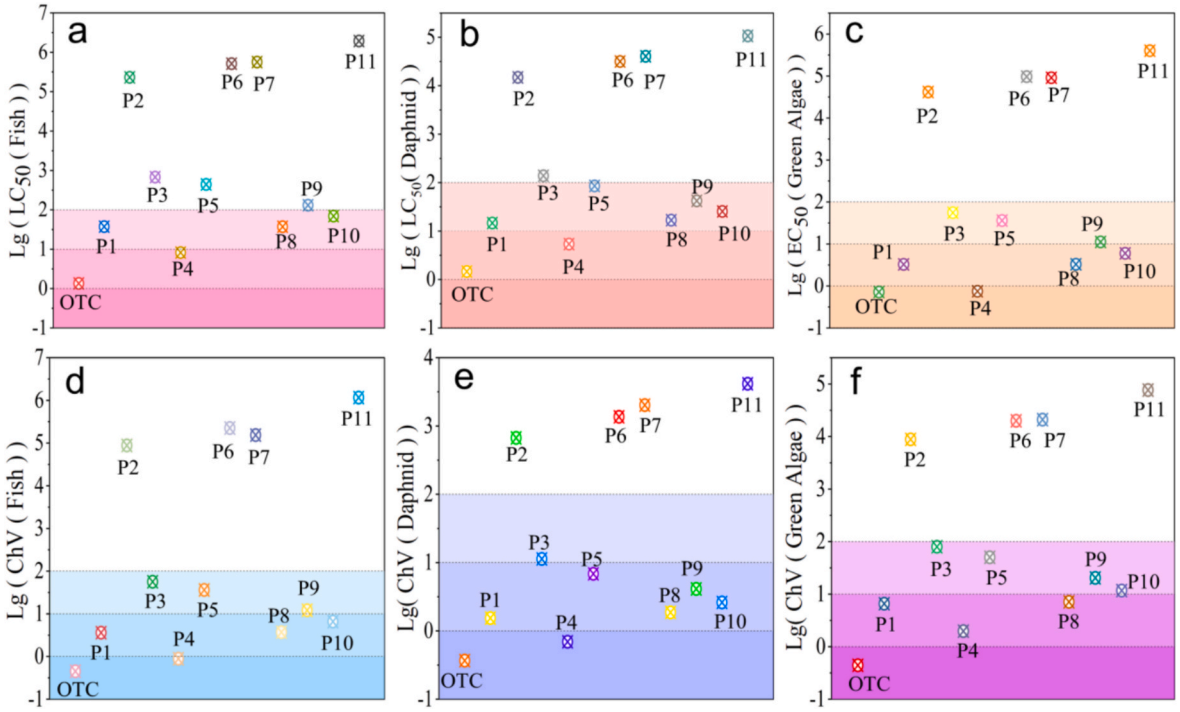

Fig. 9. a–c: the logarithmic distribution of acute toxicity; d–f: The chronic toxicity analysis.

4. Conclusions

In this study, a novel potassium ferrate (K_2FeO_4)-functionalized biochar (derived from fermented grain residues) was successfully synthesized via pyrolysis and demonstrated high catalytic efficiency in activating PI for OTC degradation in aqueous systems. The key findings can be summarized as follows:

(1) BC prepared under specific pyrolysis conditions exhibited enhanced physicochemical properties (e.g., high surface area, Fe (II)/Fe(III) redox sites, and graphitic N doping), which synergistically promoted PI activation.
(2) Under operational parameters (OTC = 20.4 mg/L, 4MBC800 = 1.1 g/L, PI = 3.3 g/L, t = 150 min), 92.1 % OTC removal was obtained within 150 min.
(3) Quenching experiments and HPLC-MS analysis confirmed that the degradation was driven by both radical ($^{\bullet}OH$, $IO_3^{\bullet}$) and non-radical ($^1O_2$) pathways, with OTC primarily undergoing hydroxylation, demethylation, and ring cleavage.
(4) The system maintained > 80 % OTC removal after 4 cycles and showed strong resistance to common water matrix interferents (e.g., NOM, Cl^-, HCO_3^-), validating its robustness for real wastewater treatment.
(5) Toxicological analysis further confirmed that the OTC degradation products generated by 4MBC/800 system exhibited no latent toxicity, demonstrating strong practical applicability.

Despite these promising results, this study has certain limitations. The catalytic performance was evaluated under controlled laboratory conditions, and its effectiveness in real industrial wastewater with more complex and variable compositions remains to be further verified. In addition, the long-term stability of the catalyst under continuous flow conditions and the economic feasibility of large-scale production and application require more in-depth assessment. Future studies should focus on pilot-scale experiments to validate the practicality and durability of the material in real wastewater treatment scenarios.

Finally, this work not only advances the design of iron-BC hybrids for PI-AOPs but also offers a sustainable waste-to-resource strategy by fermented grain residues into functional catalysts.

CRediT authorship contribution statement

Tiehong Song: Writing – original draft, Supervision, Methodology. **Ying Zhang:** Writing – review & editing, Data curation. **Hongyan Wei:** Methodology, Investigation. **Ying Wang:** Writing – review & editing, Data curation. **Yanjiao Gao:** Writing – review & editing, Software, Methodology.

Declaration of competing interest

The authors declare that they have no known competing financial interests or personal relationships that could have appeared to influence the work reported in this paper.

Acknowledgments

This work was financially supported by the Department of Science and Technology of Jilin Province, China (20240304032SF), Key Laboratory of Songliao Aquatic Environment, Ministry of Education, China (Heng 20250004), and China Northeast Municipal Engineering Design & Research Institute Co., LTD (Heng 20250147).

Appendix I

EDS spectra of various BCs

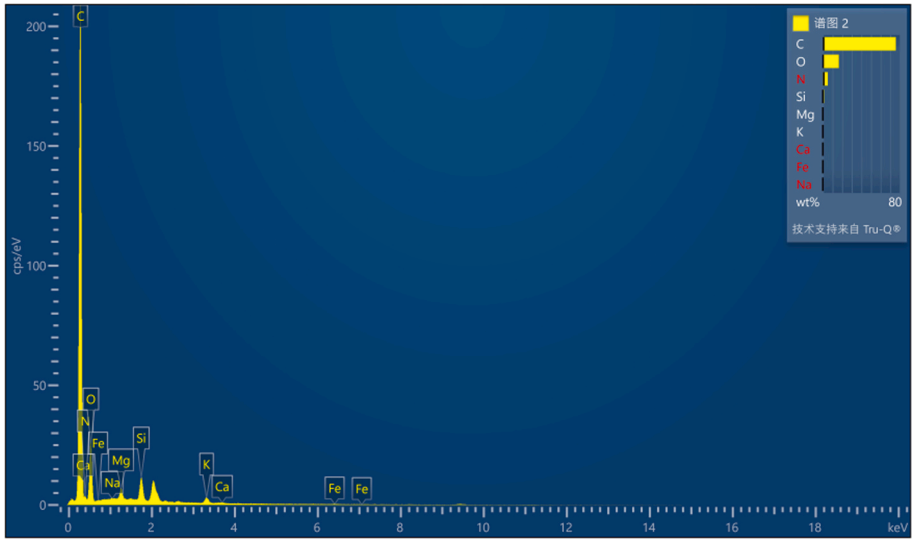

Spectrum 1. EDS spectrum of BC500

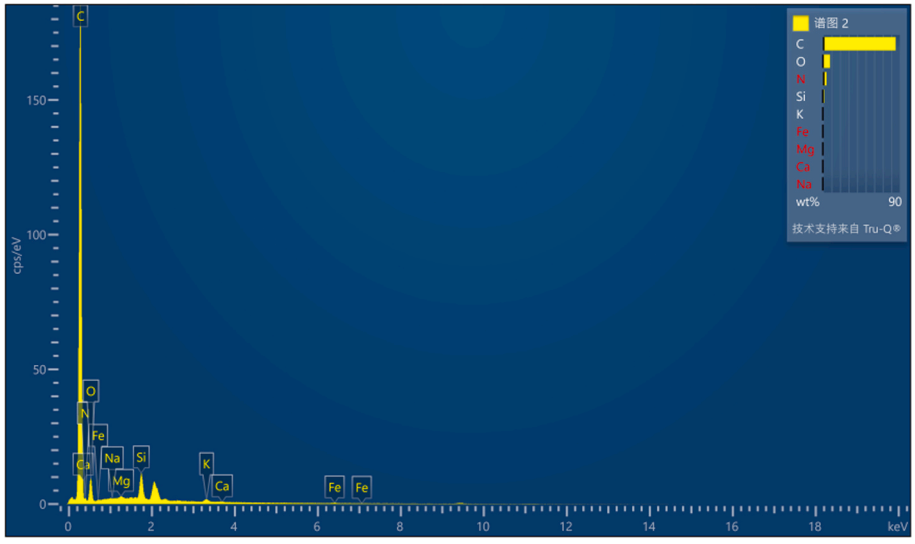

Spectrum 2. EDS spectrum of BC650

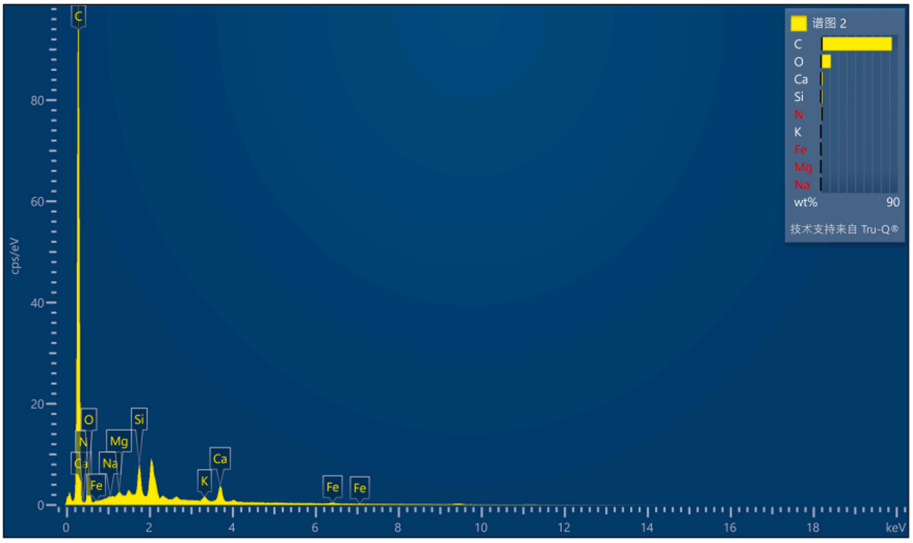

Spectrum 3. EDS spectrum of BC800

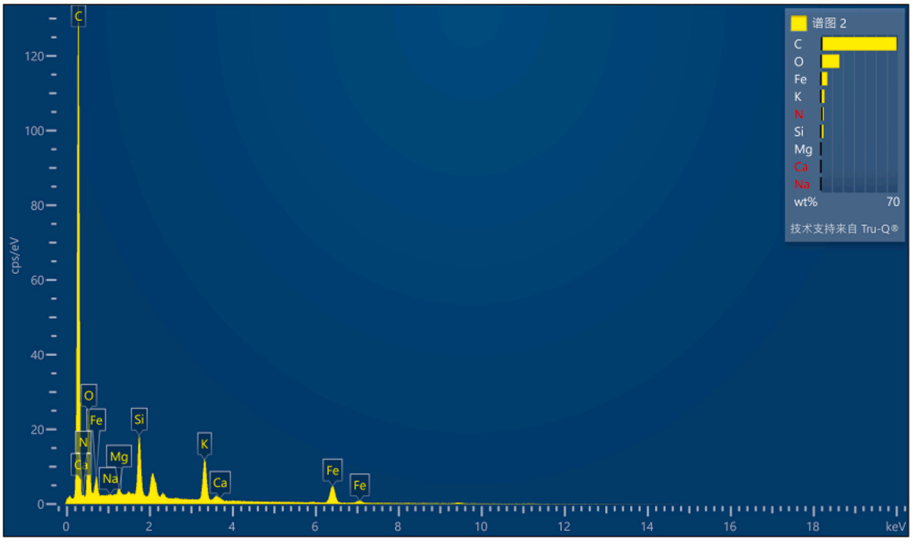

Spectrum 4. EDS spectrum of 2MBC500

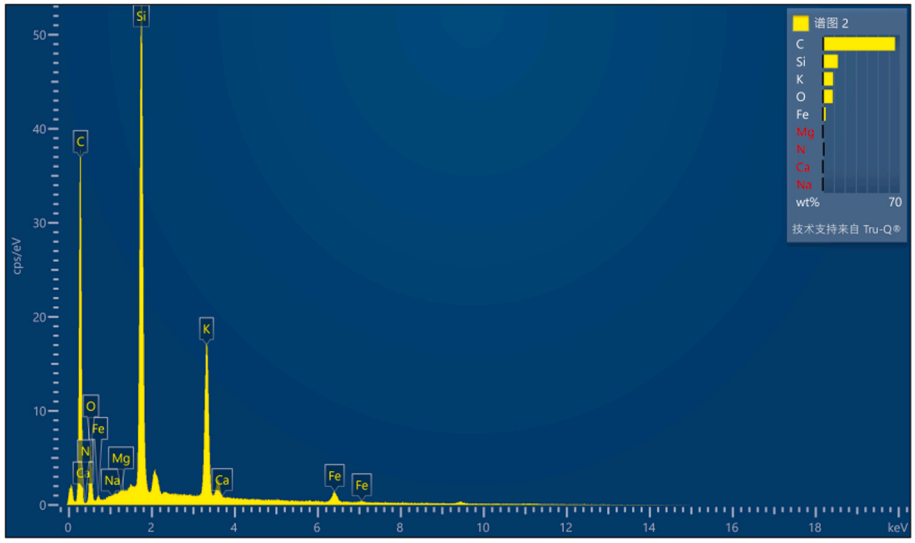

Spectrum 5. EDS spectrum of 2MBC650

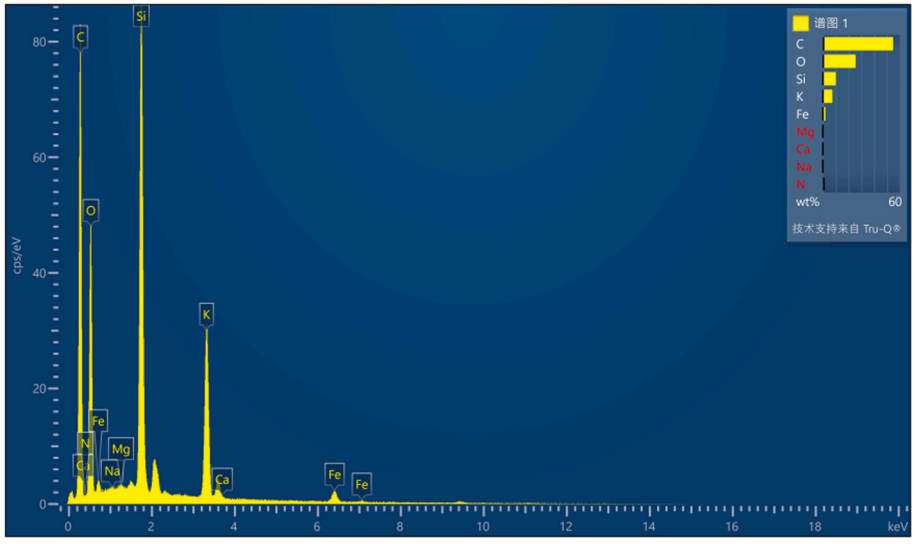

Spectrum 6. EDS spectrum of 2MBC800

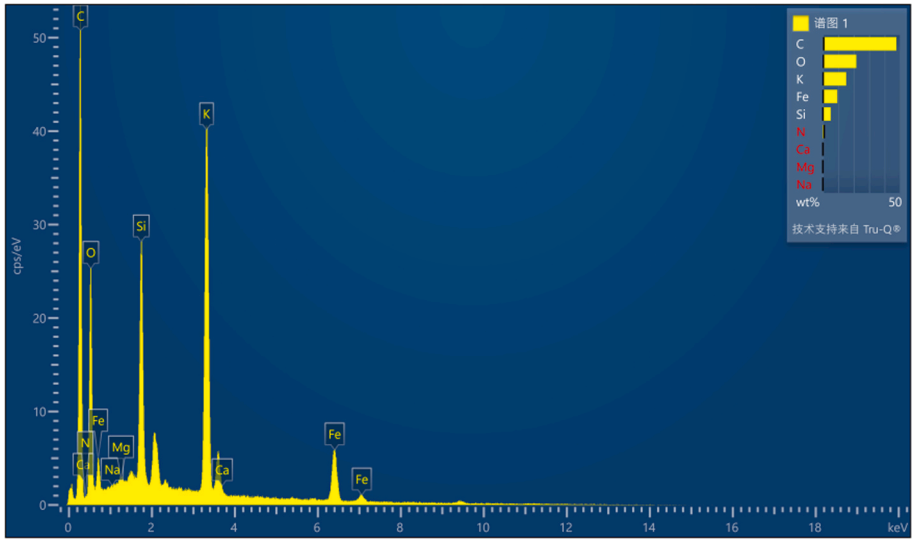

Spectrum 7. EDS spectrum of 4MBC500

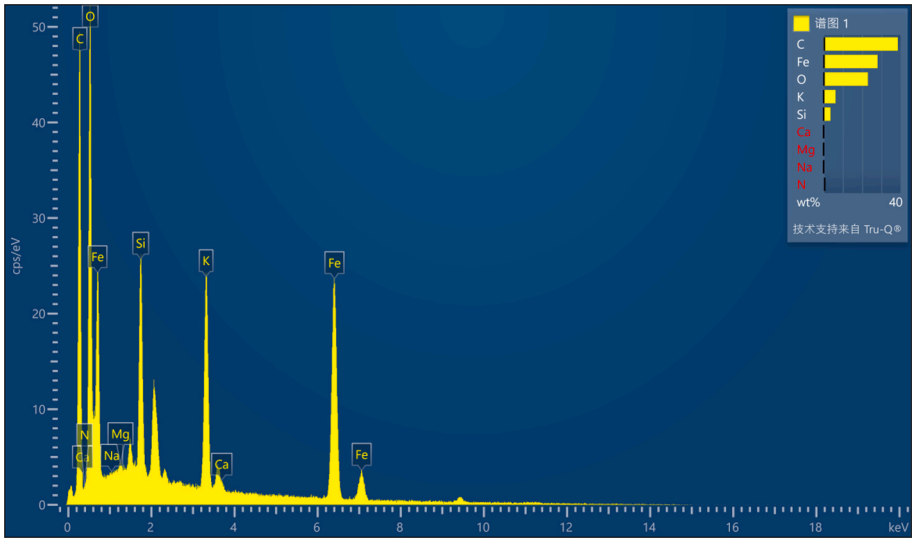

Spectrum 8. EDS spectrum of 4MBC650

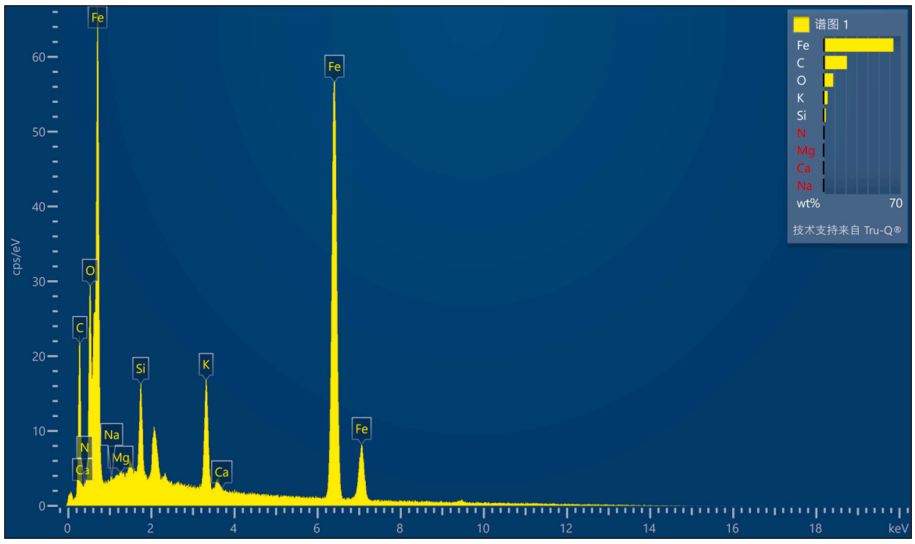

Spectrum 9. EDS spectrum of 4MBC800

References

[1] Lyu J, Yang L, Zhang L, Ye B, Wang L. Antibiotics in soil and water in China–a systematic review and source analysis. Environ Pollut 2020;266:115147.

[2] Mog M, Ngasotter S, Tesia S, Waikhom D, Panda P, Sharma S, et al. Problems of antibiotic resistance associated with oxytetracycline use in aquaculture: a review. J Entomol Zool Stud 2020;8:1075–82.

[3] Haddad MF, Abdullah BA, AlObeidi HA, Saadi AM, Haddad MF. Antibiotic classification, mechanisms, and indications: a review. Int J Med All Body Health Res 2024;5:39–46.

[4] Kolar B, Arnuš L, Jeretin B, Gutmaher A, Drobne D, Durjava MK. The toxic effect of oxytetracycline and trimethoprim in the aquatic environment. Chemosphere 2014; 115:75–80.

[5] Xie ZH, He CS, Zhou HY, Li LL, Liu Y, Du Y, et al. Effects of molecular structure on organic contaminants' degradation efficiency and dominant ROS in the advanced oxidation process with multiple ROS. Environ Sci Technol 2022;56:8784–95.

[6] Scaria J, Nidheesh PV. Comparison of hydroxyl-radical-based advanced oxidation processes with sulfate radical-based advanced oxidation processes. Curr Opin Chem Eng 2022;36:100830.

[7] Guillard C, Robert D. Catalysis in advanced oxidation technologies (AOTs) for water, air and soil treatment. Catalysts 2022;12:502.

[8] Wang JL, Xu LJ. Advanced oxidation processes for wastewater treatment: formation of hydroxyl radical and application. Crit Rev Environ Sci Technol 2012; 42:251–325.

[9] Duan X, Yang S, Wacławek S, Fang G, Xiao R, Dionysiou DD. Limitations and prospects of sulfate-radical based advanced oxidation processes. J Environ Chem Eng 2020;8:103849.

[10] Fang GD, Dionysiou DD, Wang Y, Al-Abed SR, Zhou DM. Sulfate radical-based degradation of polychlorinated biphenyls: effects of chloride ion and reaction kinetics. J Hazard Mater 2012;227:394–401.

[11] Elmitwalli T, Fouad M, Mossad M, Samy M. Periodate activation by mulukhiyah stalks and potato peels-derived biochars for the efficient degradation of sulfamethazine. J Environ Chem Eng 2024;12:112101.

[12] Li R, Wang J, Wu H, Zhu Z, Guo H. Periodate activation for degradation of organic contaminants: processes, performance and mechanism. Sep Purif Technol 2022; 292:120928.

[13] Babuponnusami A, Muthukumar K. A review on Fenton and improvements to the Fenton process for wastewater treatment. J Environ Chem Eng 2014;2:557–72.

[14] Yang L, He L, Ma Y, Wu L, Zheng L, Wang J, et al. Periodate-based oxidation focusing on activation, multivariate-controlled performance and mechanisms for water treatment and purification. Sep Purif Technol 2022;289:120746.

[15] Wang Z, Meng X, Chen K, Mitra S. High capacity aqueous periodate batteries featuring a nine-electron transfer process. Energy Storage Mater 2019;19:206–11.

[16] Madihi-Bidgoli S, Asghari F, Cheraghi S, Hamidinia H, Shagerdi E, Asadnezhad S. UV/periodate and UV/chlorine for dye degradation and real wastewater treatment: a comparative study. Water Pract Technol 2023;18:2453–68.

[17] Yue J, Guo W, Zhu Y, Li D, Liang S, Cao R, et al. Insights on the degradation mechanism of neotame using UV/periodate: roles of reactive species, kinetics, and pathways. Chem Eng J 2024;495:153059.

[18] Zeng H, Chen Y, Xu J, Li S, Wu J, Li D, et al. Iron-based materials for activation of periodate in water and wastewater treatment processes: the important role of Fe species. Chem Eng J 2024;482:148885.

[19] Li Y, Wang J, Wei Z, Li W, Duan W, Feng X, et al. Effective periodate activation by peculiar Cu2O nanocrystal for antibiotics degradation: the critical role of structure and underlying mechanism study. Appl Catal B Environ 2024;341:123351.

[20] Dou L, Huang W, Huang Y, Liu C, Li N, Li J, et al. Single-atom Ag porous tubular carbon nitride photocatalyst with N-vacancies as efficient visible-light periodate activator: performance and mechanism. Chem Eng J 2025;504:158796.

[21] Mao Y, Xu Y, Ying H. Study on the performance and mechanism of maghemite modified biochar towards periodate activation. Environ Earth Sci 2024;83:548.

[22] Yang Y, Kang Z, Xu G, Yu Y. Nitrogen and magnesium codoped biochar activates periodate to remediate bensulfuron methyl-contaminated water at low temperature: performance, mechanisms, and phytotoxicity. J Hazard Mater 2024; 480:135803.

[23] Fang G, Li J, Zhang C, Qin F, Luo H, Huang C, et al. Periodate activated by manganese oxide/biochar composites for antibiotic degradation in aqueous system: combined effects of active manganese species and biochar. Environ Pollut 2022;300:118939.

[24] Zhuo SN, Zhang W, Ren HY, Liu BF. Highly efficient degradation of acetaminophen via nano zero-valent iron biochar with periodate system at low temperature. Bioresour Technol 2024;395:130349.

[25] Xiang L, Almatrafi E, Yang H, Ye H, Qin F, Yi H, et al. Coupled carbon structure and iron species for multiple periodate-based oxidation reaction. Chem Eng J 2023; 455:140560.

[26] Wang Y, Peng W, Wang J, Chen G, Li N, Song Y, et al. Sulfamethoxazole degradation by regulating active sites on distilled spirits lees-derived biochar in a continuous flow fixed bed peroxymonosulfate reactor. Appl Catal B Environ 2022; 310:121342.

[27] Qu S, Guo W, Mou H, Wang R, Wei M, Hu X. Improvement of heterogeneous electro-Fenton oxidation of dimethyl phthalate by embedding Fe/Co bimetallic active sites into waste wine lees biochar. J Water Process Eng 2024;66:105966.

[28] Wang H, Guo W, Liu B, Wu Q, Luo H, Zhao Q, et al. Edge-nitrogenated biochar for efficient peroxydisulfate activation: an electron transfer mechanism. Water Res 2019;160:405–14.

[29] Dong X, He L, Hu H, Liu N, Gao S, Piao Y. Removal of 17β-estradiol by using highly adsorptive magnetic biochar nanoparticles from aqueous solution. Chem Eng J 2018;352:371–9.

[30] He L, Yang S, Yang L, Shen S, Li Y, Kong D, et al. Ball milling-assisted preparation of sludge biochar as a novel periodate activator for nonradical degradation of sulfamethoxazole: Insight into the mechanism of enhanced electron transfer. Environ Pollut 2023;316:120620.

[31] Li X, Jia Y, Zhou M, Su X, Sun J. High-efficiency degradation of organic pollutants with Fe, N co-doped biochar catalysts via persulfate activation. J Hazard Mater 2020;397:122764.

[32] Dai J, Wang Z, Chen K, Ding D, Yang S, Cai T. Applying a novel advanced oxidation process of biochar activated periodate for the efficient degradation of bisphenol a: two nonradical pathways. Chem Eng J 2023;453:139889.

[33] He L, Shi Y, Chen Y, Shen S, Xue J, Ma Y, et al. Iron-manganese oxide loaded sludge biochar as a novel periodate activator for thiacloprid efficient degradation over a wide pH range. Sep Purif Technol 2022;288:120703.

[34] Shaheen SM, Mosa A, Natasha AH, Niazi NK, Antoniadis V, Rinklebe J. Removal of toxic elements from aqueous environments using nano zero-valent iron-and iron oxide-modified biochar: a review. Biochar 2022;4:24.

[35] Garg S, Yuan Y, Mortazavi M, Waite TD. Caveats in the use of tertiary butyl alcohol as a probe for hydroxyl radical involvement in conventional ozonation and catalytic ozonation processes. ACS EST Eng 2022;2:1665–76.
[36] Zhu M, Lu J, Hu Y, Liu Y, Hu S, Zhu C. Photochemical reactions between 1,4-benzoquinone and O2•−. Environ Sci Pollut Res 2020;27:31289–99.
[37] Lian Q, Xu B, Yu H, Zhao J, Liu X, Sun J, et al. Determination of singlet oxygen generated in vegetable oil using furfuryl alcohol as trapping agent. Food Anal Methods 2022;15:3458–67.
[38] Hong Q, Liu C, Wang Z, Li R, Liang X, Wang Y, et al. Electron transfer enhancing Fe (II)/Fe(III) cycle by sulfur and biochar in magnetic FeS@biochar to active peroxymonosulfate for 2,4-dichlorophenoxyacetic acid degradation. Chem Eng J 2021;417:129238.
[39] Jin R, Deng C, Liu G, Zhai S, Qi D. Heterogeneous catalysis of FeOOH in-situ loaded biochar for reactive red X-3B: catalytic mechanism based on Fenton-like system. J Environ Chem Eng 2024;12:111702.
[40] Zong Y, Shao Y, Zeng Y, Shao B, Xu L, Zhao Z, et al. Enhanced oxidation of organic contaminants by iron(II)-activated periodate: the significance of high-valent iron–oxo species. Environ Sci Technol 2021;55:7634–42.
[41] Huang L, Sun Y, Wang W, Yue Q, Yang T. Comparative study on characterization of activated carbons prepared by microwave and conventional heating methods and application in removal of oxytetracycline (OTC). Chem Eng J 2011;171:1446–53.
[42] Lu G, Li X, Li W, Liu Y, Wang N, Pan Z, et al. Thermo-activated periodate oxidation process for tetracycline degradation: kinetics and byproducts transformation pathways. J Hazard Mater 2024;461:132696.